

Scaling of the supercooled dynamics and its relation to the pressure dependences of the dynamic crossover and the fragility of glass-formers

R. Casalini^{1,2} and C.M. Roland²

¹George Mason University, Chemistry Department, Fairfax VA 22030

²Naval Research Laboratory, Chemistry Division, Code 6120, Washington DC 20375-5342

(Physical Review B: submitted August 31, 2004; accepted November 23, 2004)

Abstract

Master curves of the relaxation time, τ , or viscosity, η , versus $T^{-1}V^\gamma$, where T is temperature, V the specific volume, and γ a material constant, are used to deduce the effect of pressure on the dynamic crossover and the fragility. The crossover is determined from the change in slope of derivative plots of the relaxation times or viscosities. We confirm our previous findings that the value of τ or η at the crossover is independent of both T and P ; that is, the dynamic crossover is associated with a characteristic value of the relaxation time. Previous determinations were limited to liquids having crossovers occurring at large values of τ ($> 10^{-6}$ s), whereas by interpolating within $T^{-1}V^\gamma$ space, we extend the analysis to smaller values of the crossover time. Using the superpositioned data, the dynamic crossover can be observed in isochoric data, where it is found that the relaxation time at the crossover for constant volume is equivalent to the value obtained under (the more usual) condition of constant pressure.

Similarly, from the scaling analysis, isobaric relaxation times at high pressure are deduced from experimental measurements at atmospheric pressure. We find for all glass-formers studied, that the fragility (normalized temperature dependence of τ or η) is a decreasing function of pressure. This conclusion is less subject to uncertainties in the measurements than published determinations of the pressure coefficient of fragility. Finally, we show that an empirical function, having the form of the Cohen-Grest relation but without connection to any free volume model, parameterizes the master curves, and accurately describes the data over all measured conditions.

Introduction

The topic of the glass transition has been at the center of discussions in condensed matter physics for many years. A still open question is whether the sudden, yet progressive, slowing down of the dynamical properties (viscosity, relaxation time, etc.) is due to an underlying thermodynamical transition. The glass transition temperature, T_g , is usually defined empirically, with its value depending on the thermal history of the material (cooling rate, aging, etc.), suggestive of its kinetic nature. Effectively, the glass transition corresponds to the condition whereby the material timescale becomes longer than the duration of a typical experiment. However, most theories and models consider the actual transition to occur at a different temperature, one lying either well below T_g , (and therefore not directly observable) or at some higher temperature, T_B (other subscripts may apply depending on the model). Signatures for T_B are generally difficult to observe since there is no clear discontinuity in physical properties, as might be expected for a thermodynamic transition. One manifestation of T_B is the “dynamic crossover”, which is discussed below.

A physical description of supercooled liquids currently in vogue is based on the energy landscape. In this framework, cooling of a liquid causes progressive entrapment in potential wells, so that the slowing down of the dynamics is related to a progressive decrease of available configurations. Since the energy landscape is related to intermolecular distances, in a typical isobaric measurement, the height of the potential energy barriers will change with density in a manner dependent on the “nature” of the potential. Therefore, for the isobaric temperature dependence of dynamical properties, two convoluted effects determine the number of accessible configurations: changes in thermal energy which determine the accessible region of the energy landscape, and changes of the energy landscape itself arising due to the variation of density with temperature. These convoluted effects are especially evident in materials exhibiting a strong dependence of their relaxation time on density at fixed T . This is indicative of a strong dependence of the potential energy on intermolecular distances.

A popular metric used to classify glass formers is fragility, m , usually defined as [1]

$$m = \left. \frac{d \log(x)}{d \left(\frac{T_g}{T} \right)} \right|_{T_g} \quad (1)$$

where x represents the relaxation time (τ), fluidity (η^{-1}) or other dynamical quantity. Per common usage, strong glass-formers are those having a weak dependence (small m), while for fragile liquids x has a strong dependence on T_g/T (large m). The isochoric (constant volume) fragility, m_V , is directly connected to the “shape” of the energy landscape, although this is not necessarily the case for the isobaric fragility, m_P , wherein temperature and density effects are convoluted. Herein, we elaborate on this point, by assessing differences between the two fragilities for various materials, and examining how the convolution of temperature and density effects accounts for the observed pressure dependences of the isobaric fragility.

An interesting phenomenon observed at temperatures above T_g is the dynamic crossover. When measured over many decades of frequency, a clear change is evident in the temperature dependence of various properties, including τ and η [2]. A determination of the crossover temperature is obtained using the model-independent derivative function introduced by Stickel et al. [3], which for the relaxation time is

$$\phi_r = \left[\frac{d \log(\tau)}{d(1000/T)} \right]^{-\frac{1}{2}} \quad (2)$$

Various theoretical models anticipate, or at least interpret, the dynamic crossover: (i) the liquid-liquid transition postulated for polymers by Boyer[4] (although see [5]); (ii) the crossover from free diffusion to landscape dominated diffusion at $\tau \sim 10^{-9}$ s, as predicted by the energy landscape model, first proposed by Goldstein[6]; (iii) the percolation of “liquid-like cells”, according to the Cohen-Grest free-volume model[7,8]; (iv) a marked increase in the degree of intermolecular cooperativity, according to the Coupling Model of Ngai [9, 10]; and (v) the divergence of the viscosity according to Mode Coupling Theory (MCT).[11] (Note this divergence may not actually be observed due to a transition to hopping dynamics [12]).

Recent high pressure measurements led to the discovery that the value of both the dielectric relaxation time [13] and the viscosity [14] at which the crossover occurs are independent of P and T . Using a modified Stickel function,

$$\phi_p = \left[\frac{d \log(\tau)}{dP} \right]^{-\frac{1}{2}} \quad (3)$$

a clear change of behavior is evident at a fixed value of τ or η .

More recently [15,16] we found that $\log(\tau)$ data for various T and P yield a master curve when plotted versus the parameter $T^{-1}V^\gamma$, where V is the specific volume and γ is a material-specific parameter. From an analysis of 18 glass-forming liquids and polymers, we find $0.14 \leq \gamma \leq 8.5$. These results are important both from a theoretical point of view, by offering a connection to the nature of the intermolecular potential, [15, 17, 18, 19, 20], and for practical reasons, because the superpositioned data allow predictions for conditions for which experiments may be difficult. For example, high-pressure dielectric data do not extend above 10^7 Hz, due to experimental limitations. And measurements are either isothermal or isobaric, with isochoric data having to be constructed by interpolation. However, using the general result that $\log(\tau) = \mathfrak{F}(TV^\gamma)$, the properties over a wider pressure range can be obtained, without extrapolating beyond the measured τ , the widest range of the latter invariably being for ambient pressure.

In the following, we use the $\log(\tau) = \mathfrak{F}(TV^\gamma)$ relation to reanalyze the T - and V -dependences for glass formers which have been measured under high pressure. In this manner, we can explore the consequences regarding the dynamic crossover and fragility. In particular, starting from atmospheric pressure measurements at varying temperature, we predict the isobaric behavior at any pressure \hat{P} , by finding numerically the T such that $TV^\gamma(0.1 \text{ MPa}) = TV^\gamma(\hat{P})$. In the analyses, the $V(T,P)$ behavior is described using the Tait equation of state. Similarly, the isochoric behavior at a volume \bar{V} is predicted by calculating for each value of $\log(\tau)$ the T conforming to the condition $TV^\gamma(0.1 \text{ MPa}) = T^{-1}\bar{V}^{-\gamma}$.

Results and discussion

Dynamic crossover

Phenolphthalein-dimethyl-ether (PDE). The dielectric relaxation time for PDE was measured over a broad range of temperature and pressure, at atmospheric pressure by varying temperature [21] and isothermally with varying pressure [13]. Together with the experimental determination of $V(T,P)$, we were able to show that the superpositioning condition is valid for PDE with $\gamma=4.5$; i.e., $\log(\tau) = \mathfrak{F}(TV^{4.5})$. [15] Using this result, we calculate (Fig.1) the respective temperature behaviors of τ for isochoric (solid lines) and isobaric conditions (dotted lines), using the $P = 0.1$ MPa data (points). From these calculations, it is also possible to predict the behavior at negative pressure, as shown for the isochoric curves toward the right of the isobar at 0.1 MPa. Although negative pressure is a legitimate thermodynamic condition for condensed matter, in practice obtaining data for $P < 0$ is difficult due to cavitation and others experimental limitations [22]. Note that none of the results in Fig. 1 extend beyond the range of τ which were actually measured.

Previously, we showed by calculating the function ϕ_P (eq.(3)) for isothermal measurements on PDE at elevated P , that a dynamic change occurs at the same τ_B as the crossover determined from ϕ_T (eq.(2)) for atmospheric pressure. Here, using the $\log(\tau) = \mathfrak{F}(TV^\gamma)$ relation, we extend the high pressure measurements to a more extended frequency range, in order to verify this finding by calculating the function ϕ_T for high pressure isobars. In Fig.2, the function ϕ_P is displayed for isobars both at atmospheric pressure and as calculated at 100 and 400 MPa; the temperature range of each is given in Table 1. All curves reveal the presence of a dynamic crossover. To obtain a consistent determination of τ_B , we fit lines to the high and low T ranges (solid lines), with T_B taken as their intersection (indicated by the arrow). The fitting is carried out over the same range of frequencies for each isobar. (Note that this estimate of T_B yields slightly smaller values of τ_B than the somewhat different methods

used in other publications). From the values of τ_B (Table1), it is evident that the present results confirm our previous finding that $\tau_B(T,P)$ is essentially constant for a given material.[13]

Also included in Fig.2 is the ϕ_p calculated for the isochoric curve at $V=0.7286 \text{ cm}^3/\text{g}$ (the specific volume at the ambient pressure T_g). Here again a dynamic crossover is observed; moreover, and somewhat unexpectedly, we find that τ_B is equivalent to its value for the isobaric curves. The existence of the crossover under constant volume conditions, together with its existence at constant temperature, confirms the findings that this phenomenon reflects the interplay of both thermodynamic variables.

Chlorinated biphenyl (PCB62). Dielectric relaxation times for PCB62 (a chlorinated biphenyl having 62% chlorine by weight) at various temperatures and both atmospheric and elevated pressures have been presented previously [23], and more recently, we measured the $V(T,P)$ dependence [24]. From the analysis of the PCB62 data, using either the Adam-Gibbs model [25,26,27] or the model independent function ϕ_p [13], we determined that τ_B was independent of both T and P . From the $\tau(T,P)$ and $V(T,P)$ data, the scaling $\log(\tau) = \mathfrak{F}(TV^\gamma)$ was verified, with $\gamma=8.5$. [24] Using the scaling properties, in the manner for PDE, we calculate isobars at higher pressure, as well as one isochore ($V=0.6131 \text{ ml/g}$). These are shown in Fig.3 (upper panel), along with the corresponding Stickel function (lower panel). The dynamic crossover is evident in each curve, and using the method described above for PDE, the crossover temperatures and relaxation times τ_B were obtained (Table1). For all combinations of T and P , as well as for the isochoric condition, τ_B is essentially constant, $\log(\tau_B / \text{s})=-5.9\pm 0.5$. This is somewhat less than the value estimated previously [13], due only to the different methods used to determine T_B .

Propylene carbonate (PC). Dielectric relaxation of PC has been measured at atmospheric pressure [21,28], and more recently at high pressure.[29] From the latter, τ and the ionic conductivity (σ) were found to exhibit a crossover at a characteristic value that is pressure-independent. From superposition of the relaxation times, $\gamma = 3.7$. From this, we calculate τ for high pressure over an extended frequency range, in the manner done for PDE and PCB62. Three isobars at $P = 0.3, 0.6$ and 1 GPa are displayed in Fig.4 (upper panel), together with an isochoric

curve ($V=0.7562 \text{ cm}^3/\text{g}$). The calculated ϕ_T are shown in the lower panel. T_B was determined using the same procedure described above, the results are listed with the corresponding values of $\log(\tau_B)$ in Table 1. Again, the relaxation time associated with the change in dynamics is sensibly independent of T and P , $\log(\tau_B) = -7.0 \pm 0.3$. An equivalent value is obtained for the isochoric curve.

In conclusion, from analysis using the relation $\log(\tau) = \mathfrak{Z}(TV^\gamma)$ for PDE, PCB62 and PC, we confirm our previous finding that $\tau_B(T,P) \approx \text{constant}$, with the obtained values equal to the τ_B directly measured. Thus, we can use this method to analyze other glass-formers, in which the range of the available experimental data is insufficient to probe the dynamic crossover under high pressure.

Cresolphthalein-dimethyl-ether (KDE). Dielectric relaxation times for KDE have been measured.[21,30] The material has a chemical structure very similar to that of PDE, but τ_B at atmospheric pressure is more than two decades shorter. As a result, the function ϕ_P for KDE [31] shows no indication of a change of behavior in isothermal data measured at frequencies up to 10^5 Hz. However, we can take advantage of the master curve of $\log(\tau)$ vs. TV^γ , with $\gamma = 4.5$ for KDE, to determine τ_B at elevated pressures. In the upper panel of Fig.5 are shown three isobars (experimental data for ambient pressure, along with two calculated curves) and an isochoric curve. In the lower panel is the function ϕ_T calculated for each curve. For all conditions, there is a crossover occurring at $\log(\tau_B) = -6.4 \pm 0.3$. The particular values of T_B and $\log(\tau_B)$ for each curve are listed in Table 1. These results are consistent with the absence of a crossover in high pressure measurements done at lower frequencies.

1,1'-di(4-methoxy-5-methylphenyl)cyclohexane (BMMPC). BMMPC has the largest value of the scaling exponent, $\gamma = 8.5$. Since a dynamic crossover in BMMPC is well-established [8], it is interesting to evaluate the P - and T -dependences of τ_B . A large value of γ indicates a more dominant role for volume, so we expect stronger T - and P -dependences for τ_B than for the other materials. Three isobars and an isochoric curve are shown in the upper panel of Fig.6, with the corresponding ϕ_T in the lower panel. Following the analysis described above, τ_B for BMMPC is found to be invariant to both T and P , $\log(\tau_B) = -6.1 \pm 0.5$. This invariance of τ_B is maintained

even under constant volume conditions; thus, notwithstanding the prominent role of volume in the dynamics of BMMPC, the characteristic relaxation time at the crossover is unchanged when V is maintained constant.

Salol. Salol is one of the few materials for which high pressure data are available for different experimental properties such as viscosity [32] photon correlation spectroscopy (PCS)[33] and dielectric relaxation [34] We have recently shown from dielectric relaxation measurements that $\gamma=5.2$, so it is of interest to test this scaling relation for the other experimental quantities. In Fig.7 $\log(\tau)$ from PCS [33] (lower panel) and $\log(\eta)$ [32,35] (upper panel) are plotted versus $T^{-1}V^{5.2}$. It is evident that the PCS data superpose accurately using the same γ parameter determined from dielectric relaxation. However, for the viscosity there are some deviations. While the data converge at low viscosities, a different behavior is observed for higher η . In particular, the two isotherms at the highest T seem to superpose, but they differ from the isobar at atmospheric pressure and the two lower temperature isotherms. Clearly, there is no value of γ which will yield a single master curve of the η data. The reason for this is unknown, although previously we had noted an apparent decoupling of τ and η at high pressure.[34] Given that the dielectric and photo-correlation data both superimpose for the same value of γ , it seems that further measurements are required to determine whether the breakdown of the γ -scaling for η is real. It is interesting that the $\log(\tau)$ and $\log(\eta)$ are both linear versus $T^{-1}V^{5.2}$, for τ longer than τ_B (or $\eta > \eta_B$). This would be consistent with thermally-activated (Arrhenius) behavior with and activation energy, $E_a \propto V^{5.2}$. Similar behavior has been observed for other materials. [15]

Calculating ϕ_P for the isothermal η data, a dynamic crossover is evident at the same viscosity as for the atmospheric pressure data. However, since the η in Fig.7 do not entirely superpose, this result cannot be confirmed for higher pressures. We can carry out the analysis for the dielectric results. In the upper panel of Fig. 8 is the isobar at atmospheric pressure [3], together with two isobars and an isochoric curve, all calculated using $\log(\tau)$ vs. $TV^{5.2}$. The ϕ_T calculated for each curve is shown in the lower panel, with the crossover temperature, listed in Table 1, determined from the intersection of the linear fits. From this analysis, we find $\log(\tau_B)=-6.4 \pm 0.3$ for all P, as well as for the isochoric condition.

$T_B(P)$ extracted from the dielectric data are compared to the $T_B(P)$ determined from the viscosity [14] in the inset to Fig. 8. The values are very close, confirming our previous finding, as well as the use of the $\log(\tau) = \mathfrak{I}(TV^\gamma)$ scaling for the prediction of $\tau(T,P)$. This agreement, despite the lack of superpositioning of the viscosities, likely reflects the fact that the deviation from $\log(\eta) = \mathfrak{I}(TV^\gamma)$ prevails only for $\eta > \eta_B$ (Fig.7).

-Isobaric and isochoric fragility

We can take advantage of the scaling of the relaxation times to analyze the fragility, in particular its pressure dependence and any differences for isochoric and isobaric conditions. Generally, it has been found for most of materials that m_P either decreases or is constant as pressure increases. Usually, m_P is calculated from the activation volume, ΔV^\ddagger ($= RT \partial \ln(\tau) / \partial P$), according to

$$m_P = \frac{\Delta V^\ddagger}{\frac{dT_g}{dP} R \ln(10)} \quad (4)$$

The use of this equation is subject to larger errors than a direct comparison of isobars, the latter possible through use of the scaling relation, $\log(\tau) = \mathfrak{I}(TV^\gamma)$. To avoid extrapolating, we calculate fragilities at temperatures T_α such that $\tau(T_\alpha)=10$ s. This yields a smaller value of m than using $\tau(T_g)=10^2$ s, but it does not affect the P - or V -dependences.

In Fig.9 are shown τ (measured at atmospheric pressure and calculated for $P>0.1$ MPa) for salol, PC, BMMPC, PDE , KDE and PCB62, as a function of the inverse temperature normalized by T_α . For all six materials, the fragility decreases with increasing pressure. This is shown more clearly in Fig.10, where m_P is plotted versus P . Fig.9 also includes isochoric curves, calculated for the V at which $\tau=10$ s at $P=0.1$ MPa. The values for m_V , listed in Fig.10, are all smaller than the corresponding isobaric m_P . Moreover, there is a rough positive correlation between m_P and m_V .

In light of our finding that the isobaric fragility always decreases with pressure, we reconsider 1,2-polybutadiene (PB) [36], the sole case of an m_p (determined using eq.(4)) reportedly increasing with P . The τ measured for PB for four isotherms at varying P are displayed in Fig.11 [36], along with the best fit (solid line) of the data to the empirical function [37]

$$\tau = \tau_0 \exp\left(\frac{DP}{P-P_0}\right) \quad (5)$$

where τ_0 , D and P_0 are constants. This fitting equation was employed to estimate the activation volume and the value of the pressure at which $\tau=1s$ [36]. Using the relation $\log(\tau) = \mathfrak{Z}(TV^{1.9})$ [15], we calculate isotherms for elevated pressures (shown as solid symbols in Fig.11). There is a significant difference between the values of $P(\tau=1s)$ determined from the master curve of $\log(\tau)$ versus $T^{-1}V^{-1.9}$, and those calculated via eq.(5). This is especially the case at lower temperature, where the data are scarce. These differences lead to large differences in the pressure coefficient of T_g (10% and 15% larger than dT_g/dP determined using eq.(5)). From the calculated isobars, m_p is found to decrease with P (see insert), which agrees generally with experimental data on polymers [38] (although contrary to the results reported in [36]). Thus, with the exception of the strongly H-bonded glycerol [39], fragility always decreases with pressure

The expressions for the isobaric and isochoric fragilities can be rewritten as

$$m_p = \left. \frac{\partial \log(\tau)}{\partial (Y/Y_g)} \right|_{Y_g} (1 + \gamma \alpha_p T_g) \quad (6)$$

$$m_v = \left. \frac{\partial \log(\tau)}{\partial (Y/Y_g)} \right|_{Y_g} \quad (7)$$

where $\left. \frac{\partial \log(\tau)}{\partial (Y/Y_g)} \right|_{Y_g}$ defines the slope in a normalized master curve (fragility plot with $Y (=T^{-1}V^{-\gamma})$

replacing T) [15]). It follows from the superposition relation ($\log \tau = \mathfrak{Z}(TV^\gamma)$), that the isochoric

fragility m_V is a constant. Since γ is a constant, the pressure-dependence of m_P is governed by the product of the isobaric thermal expansion coefficient and the glass temperature, and for smaller γ , this P-dependence will be smaller. Eq.(6) can be also be rewritten in terms of the ratio of the isochoric ($E_V = R \left. \frac{\partial \ln(\tau)}{\partial T^{-1}} \right|_V$) and isobaric ($E_P = R \left. \frac{\partial \ln(\tau)}{\partial T^{-1}} \right|_P$) activation enthalpies. Using the relation [15]

$$(1 + \gamma \alpha_p T_g) = \left(\frac{E_V}{E_P} \Big|_{T_g} \right)^{-1} \quad (8)$$

equation (6) becomes

$$m_P = \frac{\partial \log(\tau)}{\partial (Y/Y_g)} \Big|_{Y_g} \left(\frac{E_V}{E_P} \Big|_{T_g} \right)^{-1} \quad (9)$$

From eq. 9, a decrease of m_P with increasing pressure implies that of the ratio $E_V/E_P|_{T_g}$ is an increasing function of P . This means that at higher pressure, the relative influence of T , in comparison to V , becomes magnified. Such an inference seems to be in accord with experimental observations [20].

Recently, De Michele et al. [18] carried out simulations of a binary mixture of soft spheres interacting with an inter-particle repulsive potential, $\sim r^{3\gamma}$. They calculated diffusion constants for different degrees of “softness” of this potential ($\gamma= 6, 8, 12, 18$), and found that the isochoric fragility is independent of γ . This lack of correlation is consistent with our results herein. For example, PDE and KDE are associated with the same exponent γ , but have different fragilities. No more than a rough correlation between m_V and γ can be expected, since other factors affect the fragility. The change of fragility can be ascribed to a change in the number of available configurations. In particular, Speedy [40] derived a direct proportionality between the two quantities. Sastry [41], on the other hand, found that the fragility was proportional to the

square of the number of available configurations. A discussion of this subject can be found in [42].

Comparing the isochoric and isobaric behaviors of different materials at the same T , the isochoric τ is larger because of fewer available configurations, and it will have a weaker T -dependence, since changes in the available configurations with V are omitted. That is, the number of configurations changes only due to the possibility of exploring different parts of the energy landscape, as governed by the available thermal energy. Similarly, we note that at higher pressure, variations in τ due to the volume changes accompanying changes in T are reduced, and thus a corresponding contribution to the isobaric fragility is removed. In the limit of very high pressure, two possible scenarios are feasible: (i) $T_g \rightarrow T_g(\infty)$ and $\alpha_p \rightarrow 0$, from which it follows that $m_p \rightarrow m_v$; or (ii) $\alpha_p T_g \rightarrow \alpha_p T_g(\infty) = \text{const}$, and $m_p \rightarrow m_v(1 + \gamma \alpha_p T_g(\infty))$. The second case is supported by the fact that for many materials, at atmospheric pressure $\alpha_p T_g \sim 0.16 - 0.19$ [43]. This also accounts for the correlation we observe between m_p and m_v at atmospheric pressure. The relation between fragility and the available configurations is consistent with the independence of m_v on V . A recent calculation by Speedy [44], who assumed a form for the intermolecular potential similar to that of De Michele et al. [18], indicated that the number of available minima in the energy landscape is indeed independent of V .

-Phenomenological descriptions of $\log[\tau(Y)]$

Since the $\tau(T, V)$ behavior can be expressed as a single function of TV^γ , it is of interest to find an analytical form for this function. An obvious starting point is to consider equations which provide a good description of $\log[\tau(T)]$; that is, in the limit $\gamma \rightarrow 0$. The most common function is the Vogel-Fulcher equation [45,46]; however, it is well known that a single Vogel-Fulcher equation cannot account for the temperature behavior over the entire supercooled regime, from T_g to above T_B .

An alternative expression is the Cohen-Grest (CG) equation [7, 47]. It is one of the few equations that can describe $\tau(T)$ over a broad range, using only four adjustable parameters [8,48]. Substituting in Y^1 for T , it can be written

$$\log(\tau) = A + \frac{B}{Y^{-1} - Y_0^{-1} + \left[(Y^{-1} - Y_0^{-1})^2 + CY^{-1} \right]^{\frac{1}{2}}} \quad (10)$$

where A , B , C and Y_0^{-1} are constants.

The best fits of eq.(10) to the relaxation times of the six liquids considered herein (showing only the atmospheric pressure data for simplicity) are displayed in Fig.12, with the CG parameters listed in Table 2. The residuals are plotted in the insets. It can be seen that the deviation of the fitted curves are less than ± 0.1 over the entire range.

Although the CG equation was derived from a free-volume model of the glass transition [7,47], eq.(10) herein is an empirical modification, intended only to parameterize the $\tau(TV^\gamma)$ data. T_0 in the CG equation has been found to correspond to the crossover temperature, T_B . [8] Whether the form of eq.(10) can be linked to any theoretical model remains to be seen.

Conclusions

We have shown that master curves of the relaxation time or viscosity, having the form $\log(\tau) = \mathfrak{F}(TV^\gamma)$ can be exploited to analyze the dynamics in supercooled liquids over broad ranges of T , P and V . A functional form for the superpositioning variable is obtained by empirical modification of the CG equation (eq.(10)), without implying any connection to the free volume concepts underlying the original CG model. The focus herein is on the high frequency crossover and the dependence of the fragility on P and V . Regarding the crossover: (i) We have confirmed previous findings for PDE, PCB62, PC and salol that the crossover transpires at a fixed value of the relaxation time, τ_B (or the viscosity, η_B), independent of the particular conditions of T and P ; (ii) We have found that the dynamic crossover is evident in isochoric curves.

From analysis of temperature dependences, we find: (i) The isobaric fragility decreases with increasing pressure; this seems to be a general result for van der Waals glass-formers. (ii) The isochoric fragility is independent of pressure. (iii) The isochoric fragility is significantly less than the isobaric fragility. (iv) There is a rough correlation between the difference of between m_P and m_V and the magnitude of the scaling exponent γ . This correlation can be accounted for from eqs.(6) and (7), and considering that $\alpha_P T_g \sim 0.16-0.19$ [43]. (v) The decrease of the fragility with pressure is related to the magnitude of the increase with P in the ratio of the isobaric and isochoric activation enthalpies. These results are consistent with the idea that the fragility (and therefore the slowing down of the dynamics) is related mainly to the number of available configurations, rather than to the shape of the intermolecular potential. The latter is only one of the factors governing the configurational entropy.

References

- [1] R.Böhmer, K.L.Ngai, C.A.Angell, D.J.Plazek, J.Chem.Phys., **99**, 4201 (1993)
- [2] C.A.Angell, K.L.Ngai, G.B.McKenna, P.F.McMillan, S.W.Martin, J.Appl.Phys., **88**, 3113 (2000)
- [3] F. Stickel, E.W. Fischer, R. Richert, J. Chem. Phys. **102**, 6251 (1995)
- [4] R.F. Boyer, J. Polym. Sci. Polym. Phys. Ed **23**, 21 (1985).
- [5] D.J. Plazek, J. Polym. Sci. Polym. Phys. Ed. **20**, 1533 (1982); D.J. Plazek, G.F. Gu, *ibid* **20**, 1551 (1982); J. Chen, C.Kow, L.J. Fetters, D.J. Plazek, *ibid.***20**, 1565(1982); S.J. Orbon, D.J. Plazek, *ibid.* **20**, 1575(1982).
- [6] M. Goldstein, J. Chem. Phys. **51**, 4767(1969).
- [7] M.H. Cohen, G.S. Grest, Phys. Rev. B **20**, 1077 (1979); G.S. Grest, , M.H. Cohen, Adv. Chem. Phys. **48**, 455 (1981).
- [8] M. Paluch, R. Casalini and C.M. Roland, Phys. Rev. E **67**, 021508 (2003).
- [9] K.L. Ngai, C.M. Roland, Polymer **43**, 567 (2002).
- [10] R. Casalini, K.L. Ngai, C.M. Roland, Phys. Rev. B **68**, 014201 (2003)
- [11] W. Götze, L. Sjogren, Rep. Prog. Phys. **55**, 241 (1992)
- [12] W. Götze, J. Phys.: Cond. Matt. **11**, A1 (1999).

- [13] R.Casalini, M.Paluch, C.M.Roland, J.Chem.Phys., **118**, 5701(2003)
- [14] R.Casalini, C.M.Roland, Phys.Rev.Lett., **92**, 245702 (2004)
- [15] R.Casalini, C.M.Roland, Phys.Rev.E, **69**, 062501 (2004)
- [16] C.M.Roland, R.Casalini, Coll. Polym. Sci., **283**, 107 (2004)
- [17] M.S. Shell, P.G. Debenedetti, E. La Nave, and F. Sciortino, J. Chem. Phys. **118**, 8821 (2003)
- [18] C.De Michele, F.Sciortino, A.Coniglio, cond-matt/0405282
- [19] W.G. Hoover and M. Ross, Contemp. Phys. **12**, 339 (1971).
- [20] C. Dreyfus, A. Aouadi, J. Gapinski, M. Matos-Lopes, W. Steffen, A. Patkowski, and R.M. Pick, Physical Review E **68**, 011204 (2003).
- [21] F. Stickel, E.W. Fischer, R. Richert, J. Chem. Phys. **104**, 2043 (1996)
- [22] *Liquids Under Negative Pressure*, A.R. Imre, H.J. Maris, and P.R. Williams, eds., NATO Science Series, Vol. 84, Kluwer, Dordrecht (2002).
- [23] R.Casalini, M.Paluch, J.J.Fontanella, C.M.Roland, J.Chem.Phys., **117**, 4901(2002).
- [24] R.Casalini, C.M.Roland, J.Chem.Phys., submitted.
- [25] G.Adam, J.H.Gibbs, J.Chem.Phys. **43**, 139 (1965).
- [26] R.Casalini, S.Capaccioli, M.Lucchesi, P.A.Rolla, S.Corezzi, Phys.Rev.E **63**, 031207 (2001).
- [27] D. Prevosto, M. Lucchesi, S. Capaccioli, R. Casalini, P. A. Rolla, Physical Review B **67** 174202 (2003).
- [28] K.L.Ngai, P.Lunkenheimer, C.Leon, U.Schneider, R.Brand, A.Loidl, J.Chem.Phys., **115**, 1405 (2001)
- [29] S. Pawlus, R. Casalini, C. M. Roland, M. Paluch, S. J. Rzoska, J. Ziolo, Phys.Rev.E., in press
- [30] M.Paluch, K.L.Ngai, S.Hensel-Bielowka, J.Chem.Phys., **114**, 10872(2001).
- [31] R.Casalini, M.Paluch, C.M.Roland, J.Phys.Cond Matt., **15**, s859 (2003).
- [32] K.U.Schug, H.E.King Jr.,R.Böhmer, J.Chem.Phys.**109**,1472(1998).
- [33] L.Comez, D.Fioretto, H.Kriegs, W.Steffen, Phys.Rev.E, **66**, 032501 (2002)
- [34] R.Casalini, M.Paluch, C.M.Roland, J.Phys.Chem. A, **107**, 2369 (2003).
- [35] T. Laughlin, D.R. Uhlmann, J. Phys. Chem. **76**, 2317(1972)

- [36] C.M.Roland, R.Casalini, P.Santangelo, M.Sekula, J.Ziolo, M.Paluch, *Macromolecules*, **36**, 4954 (2003)
- [37] M.Paluch, J.Gapinski, A.Patkowski, E.W.Fischer, *J.Chem.Phys.*, **114**, 8048 (2001)
- [38] D. Huang, D.M. Colucci, G.B. McKenna, *J. Chem. Phys.* **116**, 3925 (2002).
- [39] M.Paluch, R.Casalini, S.Hensel-Bielowka, C.M.Roland, *J.Chem.Phys.*, **116**, 9839 (2002).
- [40] R.J.Speedy, *J.Phys.Chem.B*, **103**, 4060 (1999).
- [41] S.Sastry, *Nature*, **409**, 164 (2001).
- [42] G.Ruocco, F.Sciortino, F.Zamponi, C.DeMichele, T.Scopigno, *J.Chem.Phys.*, **120**, 10666 (2004).
- [43] D.W. Van Krevelen, *Properties of Polymers*, Elsevier Publ., 1997
- [44] R.J.Speedy, *J.Phys.:Condens,Matter* **15**, S1243 (2003).
- [45] H. Vogel, *Phys. Z* **22**, 645 (1921)
- [46] G.S. Fulcher, *J. Am. Ceram. Soc.* **8**, 339 (1923)
- [47] G.S. Grest and M.H. Cohen, *Phys. Rev. B* **21**, 4113 (1980); M.H. Cohen and G.S. Grest, *J. Non-Cryst. Solids* **61/62**, 749 (1984).
- [48] H.Z. Cummins, *Phys. Rev. E* **54**, 5870 (1996).

Figure Captions

Fig.1 Dielectric relaxation time for PDE. Solid lines are calculated isochoric curves for $V_1=0.72865$, $V_2=0.7380$, $V_3=0.7602$ and $V_4=0.7795$ cm³/g. Dotted lines are calculated isobaric curves for $P=100$ and 400 MPa. Points (■) are for atmospheric pressure.

Fig.2 Stickel function, ϕ_T , for dielectric relaxation time of PDE. The lines indicates the respective low and high T linear fits, done over the range $-2.27 < \log_{10}(\tau[s]) < 1.68$ and $-8.76 < \log_{10}(\tau[\sigma]) < -5.08$, whose intersection defines the dynamic crossover (values of T_B and $\log(\tau_B)$ listed in Table 1).

Fig.3 Upper panel: dielectric relaxation times for PCB62 (experimental data for 0.1MPa; other isobars and isochoric curve at $V=0.6131$ ml/g were calculated). Dotted line indicates the average of $\log(\tau_B)=-5.9$ for the different curves. Lower panel: Stickel function, with low and high T linear fits, done over the range $-5.42 < \log_{10}(\tau[s]) < 2.169$ and $-8.87 < \log_{10}(\tau[s]) < -5.98$, respectively. The vertical dotted lines in both panels represent the dynamic crossover (see Table 1).

Fig.4 Upper panel: dielectric relaxation time for PC (experimental data for 0.1MPa; other isobars and isochoric curve were calculated). Dotted line indicates the average of $\log(\tau_B)$ for the different curves. Lower panel: Stickel function, with low and high T linear fits, done over the range $-6.14 < \log_{10}(\tau[s]) < 0.63$ and $-10.21 < \log_{10}(\tau[s]) < -8.03$, respectively. The vertical dotted lines in both panels represent the dynamic crossover (see Table 1).

Fig.5 Upper panel: dielectric relaxation time for KDE (experimental data for 0.1MPa; other isobars and the isochoric curve at $V=0.7709$ ml/g were calculated). Dotted line indicates the average of $\log(\tau_B)=-6.35$ for the different curves. Lower panel: Stickel function, with low and high T linear fits, done over the range $-4.62 < \log_{10}(\tau[s]) < 2.72$ and $-9.4 < \log_{10}(\tau[s]) < -7.28$, respectively. Vertical dotted lines indicate the dynamic crossover (Table 1).

Fig.6 Upper panel: dielectric relaxation time for BMMPC (experimental data for 0.1MPa, other isobars (200 and 600 MPa) and the isochore at $V=0.9032$ ml/g were calculated). Dotted line indicates the average of $\log(\tau_B)=-6.1$ for the different curves. Lower panel: Stickel function, with low and high T linear fits, done over the range $-4.68 < \log_{10}(\tau[s]) < 3.85$ and $-8.55 < \log_{10}(\tau[s]) < -6.4$, respectively. Vertical dotted lines indicate the dynamic crossover (Table 1).

Fig.7 Upper panel: Scaled viscosity data for salol measured isothermally at high pressure [32] and at atmospheric pressure with varying temperature [35]. The dotted line corresponds to the value of η_B at the break in the derivative function ϕ_p (eq.3). Lower panel: Scaled PCS data for salol measured isothermally at high pressure [33].

Fig.8 Upper panel: Dielectric relaxation times for salol (experimental data for 0.1 MPa, calculated curves for $P = 0.3$ and 1 GPa, and $V=0.7896$ ml/g). Lower panel: Stickel functions, with linear fits over the respective ranges $-4.58 < \log(\tau[\text{s}]) < 1.6$ and $-9.59 < \log(\tau[\text{s}]) < -7.44$.

Fig.9 Isobaric dielectric relaxation times for salol, PC, BMMPC, PDE, KDE and PCB62 versus T_α/T where $\tau(T_\alpha) = 10\text{s}$. Isochors were calculated at the volume at which $\tau=10\text{s}$ at atmospheric pressure; $V=0.7907$ (salol), 0.7558 (PC), 0.9067 (BMMPC), 0.7297 (PDE), 0.7748 (KDE) and $V=0.6131$ (PCB62) ml/g.

Fig.10. Isobaric steepness index at, m_P , versus pressure, calculated from the curves in Fig.9. The lines are to guide the eyes.

Fig.11. $\log(\tau)$ versus P for 1,2-polybutadiene measured at four temperatures. Open symbol are experimental data, solid symbols were calculated from data at atmospheric pressure using $\log(\tau) = \mathfrak{I}(TV^{1.9})$. Solid lines represent fits to eq.(5). The insert shows the m_P calculated from the isotherms using $\log(\tau) \propto TV^{1.9}$.

Fig.12. $\log(\tau)$ versus $T^{-1}V^{-\gamma}$ for the six materials studied herein, along with the best fit of eq.(10). The fit parameters are given in Table 2. The residuals are plotted in the insets.

Table captions

Table 1 Results from analysis of dielectric relaxation data for several materials. The T_B were determined from the intersection of the two linear fits, and τ_B is the corresponding value of relaxation time.

Table 2 Best fit parameters of the dielectric relaxation times to eq.(10)

Material		range of T [K]	T_B [K]	log(τ_B [s])
<i>PDE</i>	Isobar 0.1 MPa	295.0 - 415.1	321.7±9	-3.9±1.5
<i>PDE</i>	Isobar 100 MPa	320.5 - 460.8	349.7±9	-3.6±0.8
<i>PDE</i>	Isobar 400 MPa	384.6- 561.8	421.8±11	-3.8±1
<i>PDE</i>	Isochoric 0.7285 ml/g	295.0 - 589.9	345±10	-3.7±0.8
<i>PCB62</i>	Isobar 0.1 MPa	268.1-377.4	315.5±8	-5.9±1
<i>PCB62</i>	Isobar 200 MPa	323.5-498.5	393.7±6	-5.9±0.9
<i>PCB62</i>	Isobar 600 MPa	381.7-662.2	480.7±10	-5.9±1
<i>PCB62</i>	Isochoric 0.6131 ml/g	259.5-690.1	393±10	-5.8±0.9
<i>PC</i>	Isobar 0.1 MPa	159.1-276.0	188.6±7	-7±0.9
<i>PC</i>	Isobar 300 MPa	183.7-336.9	221.3±9	-6.9±.6
<i>PC</i>	Isobar 600 MPa	204.5-383.4	247.5±10	-7.0±1
<i>PC</i>	Isobar 1 GPa	228.3-433.5	277.7±11	-6.9±0.7
<i>PC</i>	Isochoric 0.7562 ml/g	159.1-382.4	202.9±8	-7.2±0.7
<i>KDE</i>	Isobar 0.1 MPa	307.7-478.9	373.9±10	-6.4±0.8
<i>KDE</i>	Isobar 400 MPa	386.1-678.4	506.9±12	-6.4±0.6
<i>KDE</i>	Isobar 1 GPa	523.0-880.0	653.8±16	-6.4±0.6
<i>KDE</i>	Isochoric 0.7562 ml/g	307.7-827.8	452.7±13	-6.3±0.4
<i>BMMPC</i>	Isobar 0.1 MPa	259.1-359.7	315.4±10	-6.2±0.9
<i>BMMPC</i>	Isobar 200 MPa	306.4-442.1	377±19	-6.0±1
<i>BMMPC</i>	Isobar 600 MPa	383.4-565.9	480±22	-6.1±1
<i>BMMPC</i>	Isochoric 0.9032 ml/g	259.2-613.5	422±40	-6.2±1
<i>Salol</i>	Isobar 0.1MPa	219.3-315.4	253.2±5	-6.3±0.7
<i>Salol</i>	Isobar 300 MPa	268.2-409.5	315.4±6	-6.3±0.7
<i>Salol</i>	Isobar 600 MPa	308.8-491.2	372.1±7	-6.6±0.5
<i>Salol</i>	Isochoric 0.9032 ml/g	219.1-458.1	290.2±5	-6.3±0.3

Table 1 Casalini and Roland

Material	γ	A	B [Kml^γg^{-γ}]	C [Kml^γg^{-γ}]	Y₀⁻¹ [Kml^γg^{-γ}]
<i>PDE</i>	4.5	-9.90±0.04	154.2±5.8	6.27±0.09	81.1±0.6
<i>PC</i>	3.7	-11.161±0.008	150.4±1.4	3.42±0.05	57.69±0.19
<i>KDE</i>	4.5	-10.4±0.01	291.6±4	17.95±0.1	122.6±0.5
<i>BMMPC</i>	8.5	-10.2±1.4	393±294	44±27	170.3±12.8
<i>salol</i>	5.2	-10.74±0.01	125.6±2.5	7.21±0.07	82.0±0.4
PCB62	8.5	-9.49±0.03	5.5±0.3	0.79±0.03	7.19±0.03

Table 2 Casalini and Roland

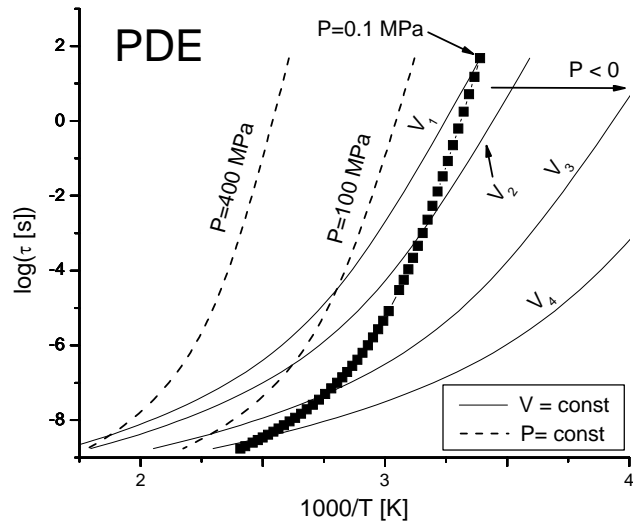


Fig. 1: Casalini and Roland

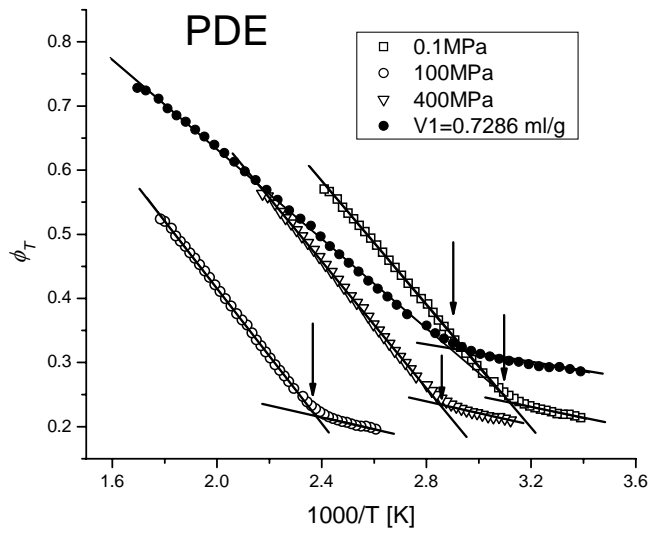


Fig.2 Casalini and Roland

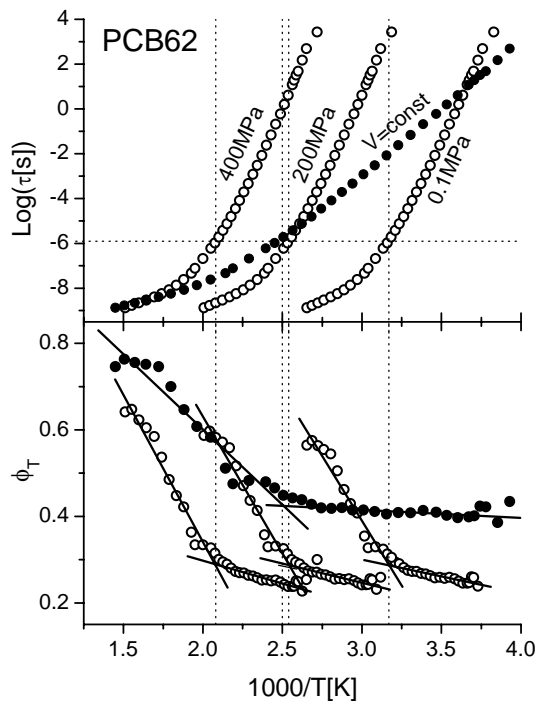


Fig.3 Casalini and Roland

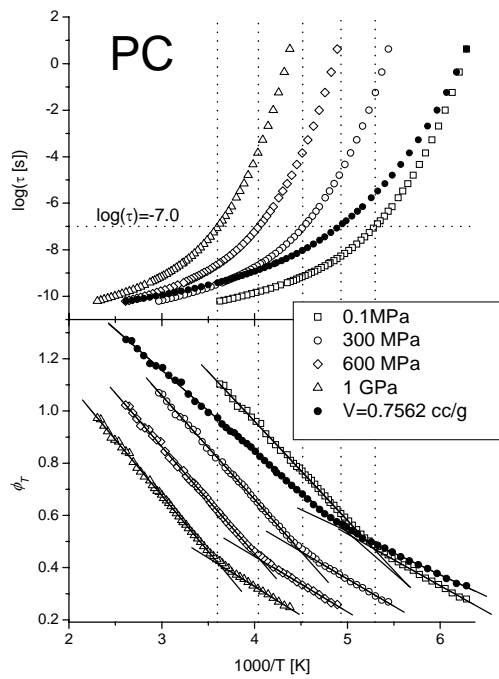


Fig.4 Casalini and Roland

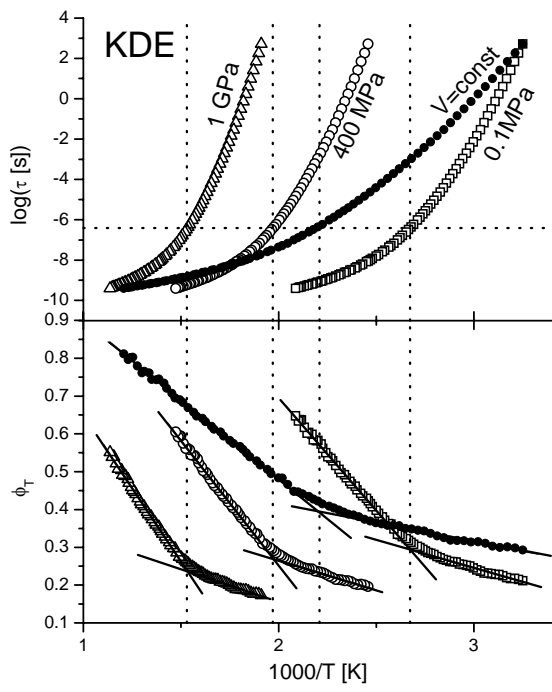


Fig.5 Casalini and Roland

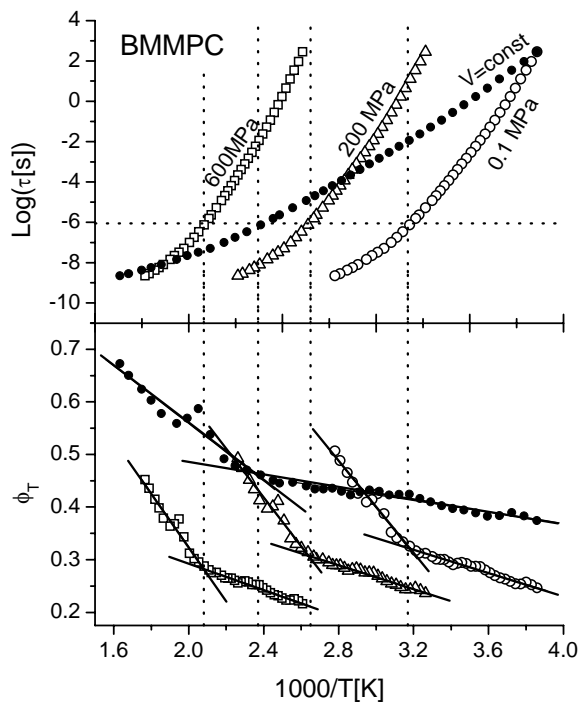


Fig.6 Casalini and Roland

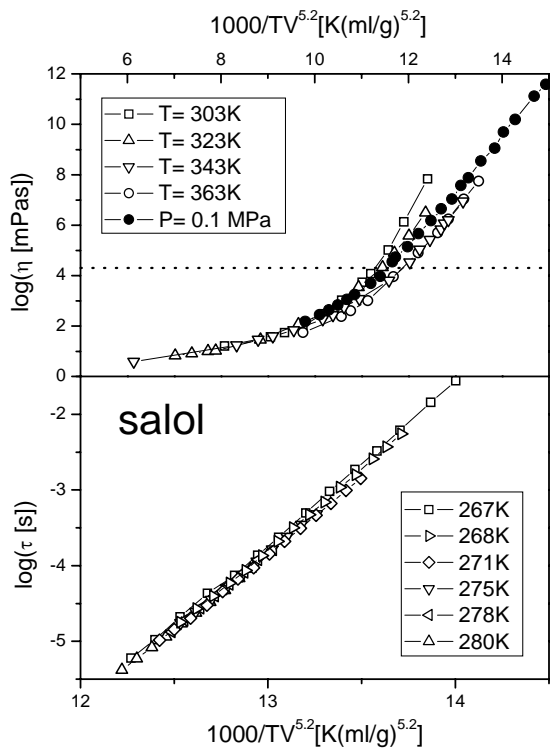


Fig.7 Casalini and Roland

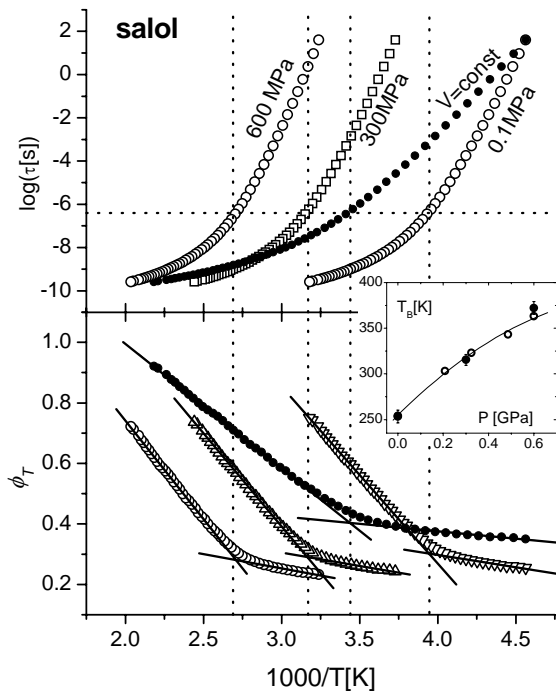


Fig.8 Casalini and Roland

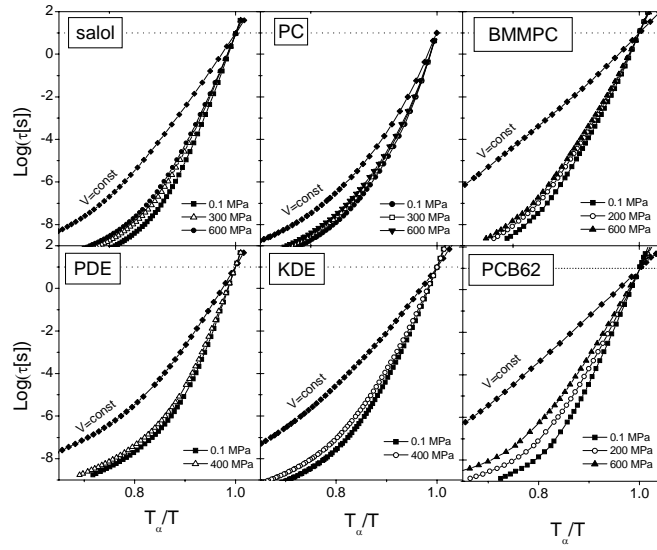


Fig.9 Casalini and Roland

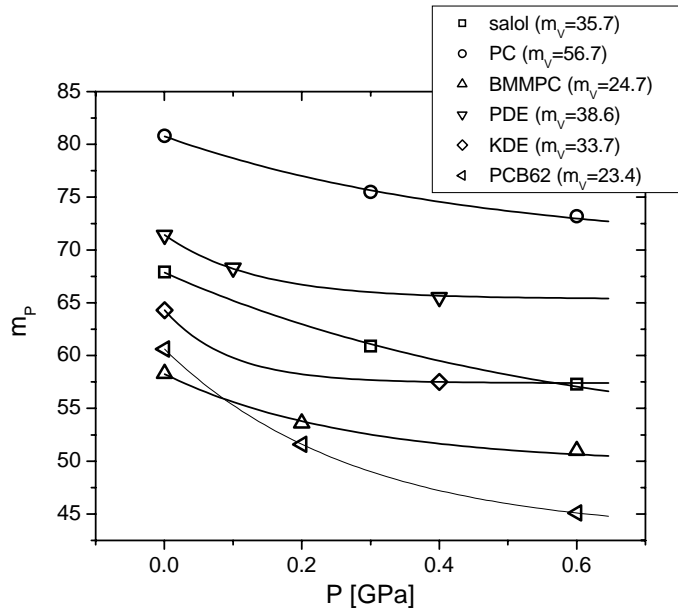


Fig.10. Casalini and Roland

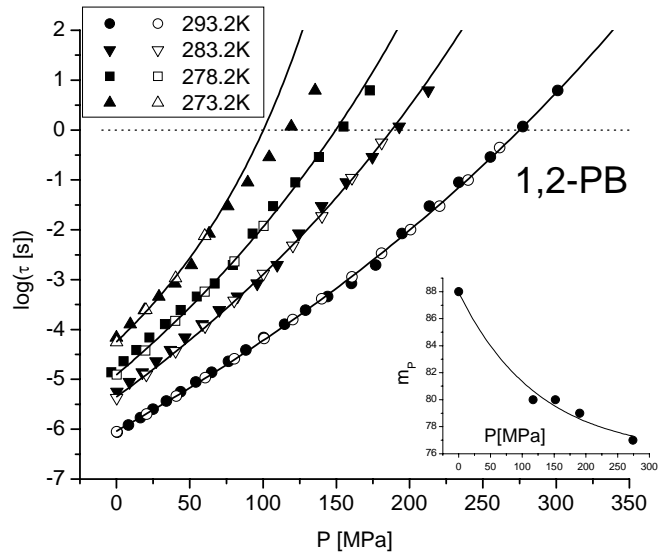


Figure 11. Casalini and Roland

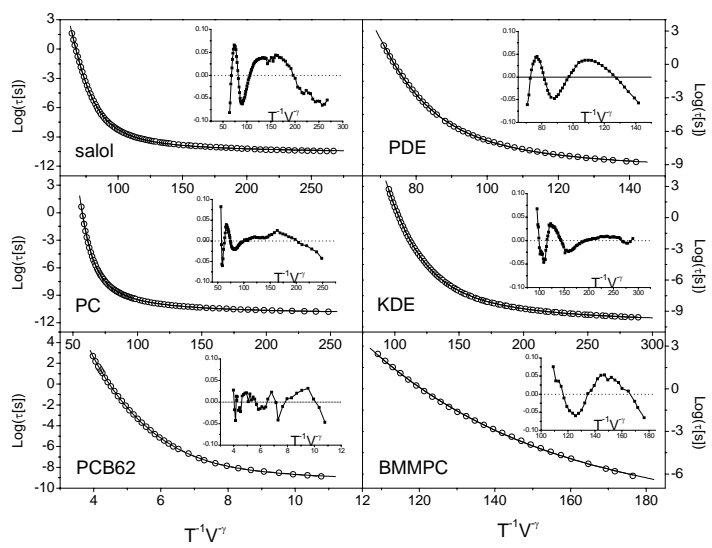


Fig.12 Casalini and Roland